Anisotropic Third-Moment Estimates of the Energy Cascade in Solar Wind Turbulence Using Multispacecraft Data

K. T. Osman, M. Wan, W. H. Matthaeus, J. M. Weygand, and S. Dasso

Phys. Rev. Lett. **107**, 165001 — Published 10 October 2011

DOI: 10.1103/PhysRevLett.107.165001

Anisotropic Third-Moment Estimates of the Energy Cascade in Solar Wind Turbulence using Multi-Spacecraft Data

K.T. Osman,[1,*] M. Wan,[1] W.H. Matthaeus,[1] J.M. Weygand,[2] and S. Dasso[3]

[1] *Bartol Research Institute, Department of Physics and Astronomy, University of Delaware, DE, USA.*
[2] *University of California, Institute for Geophysics and Planetary Physics, Los Angeles, CA, USA.*
[3] *Instituto de Astronoma y Fsica del Espacio (CONICET-UBA) and Departamento de Fsica (FCEN-UBA), Buenos Aires, Argentina.*

(Dated: August 24, 2011)

The first direct determination of the inertial range energy cascade rate, using an anisotropic form of Yaglom's law for magnetohydrodynamic turbulence, is obtained in the solar wind with multi-spacecraft measurements. The two-point mixed third-order structure functions of Elsässer fluctuations are integrated over a sphere in magnetic field-aligned coordinates, and the result is consistent with a linear scaling. Therefore, volume integrated heating and cascade rates are obtained that, unlike previous studies, make only limited assumptions about the underlying spectral geometry of solar wind turbulence. These results confirm the turbulent nature of magnetic and velocity field fluctuations in the low frequency limit, and could supply the energy necessary to account for the non-adiabatic heating of the solar wind.

PACS numbers:

Turbulence is a universal nonlinear fluid phenomenon which acts to transfer dynamical energy between scales. The solar wind provides a natural laboratory for the in situ study of plasma turbulence, where the framework of magnetohydrodynamics (MHD) has been successful in describing magnetic and velocity field fluctuations at scales above the ion inertial length [see e.g. 1, and references therein]. Here the large-scale magnetic field orders the fluctuations [2], breaking the directional symmetry familiar in hydrodynamics. It induces anisotropy, e.g., in the wave vector distribution of energy, a feature of plasma turbulence seen in theoretical models [3], numerical simulations [4], and solar wind observations [5]. These studies suggest anisotropy is important even for moderate strength mean magnetic fields, thus influencing any plasma property that depends on the three-dimensional structure of the turbulence.

The Kolmogorov-Yaglom law for the third-order longitudinal structure functions [6, 7] is fundamental in characterizing the energy cascade in incompressible hydrodynamics [8]. Extension of this law to time-stationary incompressible homogeneous MHD turbulence [9, 10] implies two symmetric scaling laws expressed in terms of Elsässer variables $\mathbf{z}^{\pm} = \mathbf{v} \pm \mathbf{b}$, namely

$$\nabla \cdot \left\langle \delta \mathbf{z}^{\mp} \left| \delta \mathbf{z}^{\pm} \right|^2 \right\rangle = -4\epsilon^{\pm}, \tag{1}$$

where the magnetic field fluctuations are in velocity units, $\delta \mathbf{z}^{\pm} = \mathbf{z}^{\pm}(\mathbf{x} + \delta\mathbf{x}) - \mathbf{z}^{\pm}(\mathbf{x})$ are the increments of the Elsässer fields, and $\epsilon^{\pm}$ are the respective energy dissipation rates. An ensemble average is denoted by $\langle \ldots \rangle$. This differential form of the third-order law makes no assumptions about the underlying spectral geometry of MHD turbulence. The existence of the third-order law can be considered more fundamental than the phenomenologies usually associated with the second order moment. This is partly because second-order statistical phenomenologies are derived using techniques such as dimensional analysis. In contrast, the third-order law is a precise conclusion deriving from the MHD equations that only assumes some basic symmetries in time and space. Interpretation in terms of energy cascades and heating rates is neither determined by, nor discriminates between, the plethora of spectral laws obtained from phenomenological models. Indeed, understanding the mixed third-order moment, and higher order statistics in general, could lead to a more unified, if not unique, description of MHD turbulence.

Energy cascade rates in solar wind turbulence have been obtained from single spacecraft estimates of the third-order law. These studies almost invariably assume an isotropic geometry [11–13]:

$$\left\langle (\hat{\mathbf{r}} \cdot \delta \mathbf{z}^{\mp}) \left| \delta \mathbf{z}^{\pm} \right|^2 \right\rangle = -\frac{4}{3}\epsilon^{\pm} |\mathbf{r}| \,. \tag{2}$$

There have also been studies which included simple models of anisotropy [14, 15], and while such prescriptions are useful paradigms, they are nonetheless restrictive and do not represent the full spectral anisotropy of the solar wind plasma. Comparison between these studies is complicated by the use of data sets which differ in size, heliolatitude, and heliocentric distance. Hence, it is not clear how the neglect of anisotropy affected these results or contributed to the possible inconsistencies between studies [16–19]. In advance of a full and detailed analysis based on Eq. (1), it is also unclear how to assess the accuracy of various theoretical formulations of the axisymmetric third-order relation [e.g. 20–23].

Here we adopt a multi-spacecraft technique [24, 25] to estimate the third-order law, based only upon Eq. (1) and allowing for arbitrary axisymmetric rotations about the mean magnetic field direction. A pair of spacecraft,

separated by a distance $\mathbf{d}_{12}$, in a fast moving plasma will measure Elsässer field time series $\mathbf{z}_1^{\pm}(t)$ and $\mathbf{z}_2^{\pm}(t)$ along the flow direction. If the sampling time of solar wind fluctuations is much less than the characteristic time scale on which they vary, each separate spacecraft time series satisfies Taylor's hypothesis [26] and can be considered a spatial "snapshot" of the plasma. For multiple spacecraft, this condition is satisfied when [27]

$$\frac{v_{sw}\Delta t}{|\mathbf{d}_{12} - \mathbf{v}_{sw}\Delta t|} \cdot \frac{v_A}{v_{sw}} \ll 1, \tag{3}$$

where v_{sw} is the solar wind flow speed, v_A is the Alfvén speed, and $|\ldots|$ denotes a vector magnitude. This is the condition for the single spacecraft case ($v_{sw} \gg v_A$) multiplied by the ratio of the scale on which variations are measured in the plasma frame to the spatial separation between the spacecraft. In configurations where the spacecraft separation is smaller than the typical sampling scale, Taylor's hypothesis is less well satisfied than the single spacecraft case. In practice, this condition is well satisfied in the solar wind for most time lags, Δt. Any time lags that result in the left side of Eq. (3) being greater that 0.3 are considered not to satisfy Taylor's hypothesis and are removed. Hence, the spacecraft time series are equivalent to spatial series in the plasma frame: $z_1^{\pm}(-\mathbf{v}_{sw}t)$ and $z_2^{\pm}(\mathbf{d}_{12}-\mathbf{v}_{sw}t)$. Varying the time lag corresponds to changing the vector separation between each pair of sampling points in the plasma frame:

$$\mathbf{r}(\Delta t) = \mathbf{d}_{12} - \mathbf{v}_{sw}\Delta t. \tag{4}$$

Hence, in contrast to single spacecraft studies, a range of scales and angular dependences of the mixed third-order moment can be sampled using only a single data interval.

We use 4 s resolution spin averaged magnetic and velocity field data from the FGM [28] and CIS HIA instruments [29] on board the Cluster 1 and 3 spacecraft. The intervals of data used are at least an hour in duration and were taken from the period 2006 January–March when the Cluster spacecraft were in the solar wind at separations around 10,000 km, which is in the inertial range.

A magnetic field aligned right handed orthogonal coordinate system is used to identify anisotropies. The z-axis is aligned with the mean magnetic field direction, the x-direction is in the plane defined by the mean magnetic field and solar wind velocity (nearly radial) vectors, and the y-axis completes the right handed system. In addition, a field angle θ_{SB} is defined as the acute angle between the time-lagged spacecraft separation vector and the field direction. Good coverage in θ_{SB} is needed to accurately evaluate Eq. (1) integrated over a sphere[22],

$$\int_0^{\pi/2} \left\langle F^{\pm} \right\rangle \sin\theta_{SB} d\theta_{SB} = -\frac{4}{3}\epsilon^{\pm} |\mathbf{r}|, \tag{5}$$

where $F^{\pm} = (\hat{\mathbf{r}} \cdot \delta\mathbf{z}^{\mp}) |\delta\mathbf{z}^{\pm}|^2$ is the flux density, and the Elsässer variables have been sector rectified [30] such that $\mathbf{z}^+$ is sunward and $\mathbf{z}^-$ is anti-sunward. We assume axisymmetry about the mean magnetic field which allows all the unique information to be captured within a single quadrant. Note that prior applications of the third-order law to the solar wind have, in effect, frequently assumed that the bracketed quantity in the integrand of Eq. (5) can be brought outside the integral. This can only be justified for isotropic turbulence.

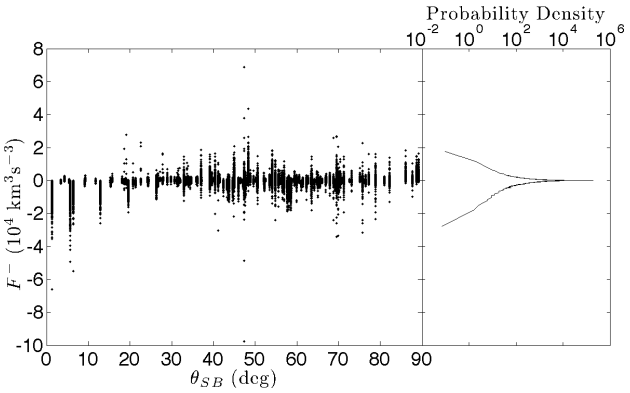

FIG. 1: All estimates of the anti-sunward normalized flux density with the corresponding PDF, both highlighting the almost symmetrical character of the mixed third-order statistic. There is good θ_{SB} coverage, but it is non-uniform: sparser parallel and perpendicular to the mean magnetic field direction, $\theta_{SB} = 0$–10° and $\theta_{SB} = 80$–90°. The smoothness of the PDF, where each bin contains around 100 data points, implies that the associated statistical quantities are well defined.

The multi-spacecraft technique is used to compute time-lagged estimates of $F^{\pm}$ in the range $\mathbf{r} = 1.1 \pm 0.1 \times 10^4$ km, which has the greatest θ_{SB} coverage. These spatial lags all lie well within the inertial range of solar wind turbulence. Flux density values obtained from each time interval are normalized by $\sigma_{\mp}\sigma_{\pm}^2$, where $\sigma_{\pm}^2 =< (\mathbf{z}^{\pm} - < \mathbf{z}^{\pm} >)^2 >$, so that these results can be combined. Figure 1 shows all the estimates of F^- that are used in this analysis, and the corresponding probability distribution function (PDF). The PDF is smooth, indicating that the statistical quantities associated with this study are well defined. Similar results are obtained for F^+. It should be noted that the difficulty in obtaining a statistically robust estimate of the third-order law is, in part, due to the almost symmetrical character of the PDFs of flux density. However, the PDF in Fig. 1 does indicate a slight skewness towards negative values — this is required for a physical interpretation of Eq. (5).

Figure 1 shows that there is good coverage in θ_{SB}, but it is not uniform. Therefore, the data is binned and averaged such that each bin contains at least 10,000 flux density estimates, and $d\theta_{SB}$ in Eq. (5) corresponds to the bin widths. The left hand side of Eq. (5) is obtained by summing these bins for, separately, the sunward and anti-sunward third-order laws. This procedure provides an estimate of each dissipation rate $\epsilon^{\pm}$, after dividing out

the separation distance and the constant factor. From this analysis at 10,000 km separation, where spherical symmetry was not assumed, the inertial range cascade rates are $\epsilon^+ = 5.2 \times 10^3$ Jkg^{-1}s^{-1} and $\epsilon^- = 5.7 \times 10^3$ Jkg^{-1}s^{-1} — see Table I for error estimates.

TABLE I: Energy cascade rates and their associated errors, obtained from the full differential form of the third-order law.

	$\epsilon \pm \sigma_\epsilon$ (10^2 Jkg^{-1}s^{-1})	
$\lvert\mathbf{r}\rvert$ (10^3 km)	Outward	Inward
4.2	60 ± 3	49 ± 2
11.1	57 ± 2	52 ± 3

The accuracy of these cascade rates can be corroborated with additional independent estimates. To this end, the analysis is repeated for spacecraft separations around 4,000 km, during the period 2003 January–March. This provides a second pair of $\epsilon^\pm$ estimates based on Eq. (5), where the angular coverage is similar to that shown in Fig. 1. Indeed adequacy of coverage is a condition for selecting the range employed. The resulting cascade rates are (see Table I) $\epsilon^+ = 4.9 \times 10^3$ Jkg^{-1}s^{-1} and $\epsilon^- = 5.8 \times 10^3$Jkg^{-1}s^{-1}.

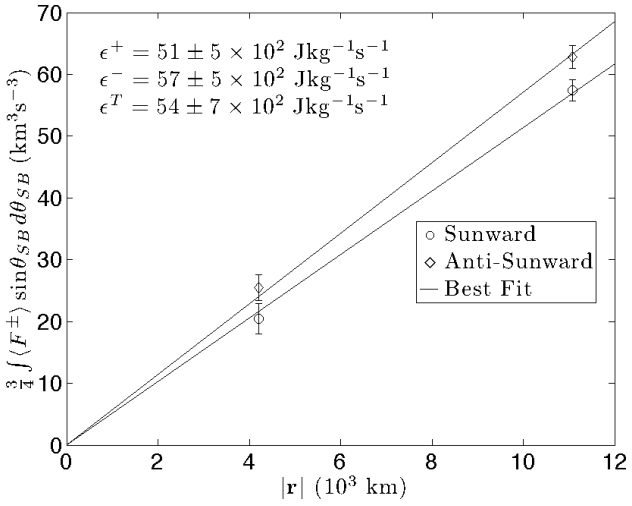

FIG. 2: Linear scaling of the (squares) sunward and (circles) anti-sunward components of the third-order law. The dashed lines are least squares fits to the data that have the added restriction of passing through the origin. It is the gradients of these lines that correspond to the mean volume averaged cascade rates. The total energy transfer rate, which becomes the dissipation rate at small scales, is the average of the sunward and anti-sunward components.

Here we recall from Eq. (5) that the integrated flux density should scale linearly with spatial separation. Indeed, previous observations within the solar wind have all measured this scaling [11, 15]. The present study makes only limited assumptions about the spectral geometry of MHD turbulence, which should only strengthen the underlying linear scaling. Hence, each pair of third-order law estimates (Table I) is fitted to a least squares line that must pass through the origin. Figure 2 shows this linear scaling of the third-order law. It should be noted that data limitations mean the possibility of alternatives to linear scaling cannot be completely excluded. However, the two estimates of the third-order law (near 4,000 km and 10,000 km) both fall, within errors, on the same line through the origin. This has not in any way been guaranteed by the methodology adopted, and is consistent with the presence of linear scaling. The gradients of the best-fit lines correspond to the sunward and anti-sunward energy transfer rates in solar wind turbulence, based on the data at both computed separations. These values are $\epsilon^+ = 51 \pm 5 \times 10^2$ Jkg^{-1}s^{-1}, $\epsilon^- = 57 \pm 5 \times 10^2$ Jkg^{-1}s^{-1}, and the total dissipation rate $\epsilon_T = 54 \pm 7 \times 10^2$ Jkg^{-1}s^{-1} which is broadly consistent with previous studies conducted in the ecliptic plane [14].

TABLE II: Energy cascade rates and their associated errors for different spectral geometries and heliolatitudes. The first entry corresponds to the results obtained from the full differential form of the third-order law, with the assumption of axisymmetry. The remaining entries were all obtained using single spacecraft analysis techniques [13, 14].

		$\epsilon \pm \sigma_\epsilon$ (10^2 Jkg^{-1}s^{-1})		
Geometry	Latitude	Outward	Inward	Total
Full 3D	Ecliptic	57 ± 5	51 ± 5	54 ± 7
Isotropic	Ecliptic	105 ± 2	25 ± 1	65 ± 1
2D + 1D	Ecliptic	140 ± 3	18 ± 3	79 ± 2
Isotropic	Poles	1.8 ± 0.7	1.6 ± 0.5	1.7 ± 0. 9

We have used the full differential form of the third-order structure function law for MHD turbulence, with the assumption of axisymmetry, to estimate the cascade rates associated with the two Elsässer energies. Table II lists the values obtained from our multi-spacecraft analysis and, for comparison, estimates obtained from previous single spacecraft studies. While the listed results are broadly consistent, there are significant differences. In particular, we find the sunward and anti-sunward cascade rates are, within errors, equal to each other. This is consistent with the view of cross-helicity and energy decay that has emerged from some theoretical treatments [e.g. 31, 32]. However, these results have not been corroborated by other in-ecliptic studies. This could be because the simple spectral models previously used are not accurate representations of the complex anisotropies exhibited by the Elsässer fluctuations. Since we do not make such restrictive assumptions, not only is our approach more fundamental, it also provides more accurate estimates of the energy transfer rates. Note that inherent in our methodology is the use of a large number of data intervals. Therefore, it is possible that different underlying spectral conditions have been averaged in such a way as to undermine the influences of anisotropy. However, the

robustness of our results suggests that this is unlikely.

The observed existence of the third-order law scaling confirms the turbulent nature of the solar wind magnetic and velocity field fluctuations in the low frequency limit of magnetohydrodynamics. An active MHD turbulence cascade can provide the additional heat required to explain the non-adiabatic temperature profile of the solar wind [e.g. 33]. We have estimated the total turbulence cascade rate, which can be considered the volume averaged dissipation rate, and it is instructive to ascertain if the cascade can account for the solar wind heat budget. [34] derived an expression for the proton heating at 1 AU:

$$\epsilon_{heat} = 3.6 \times 10^{-5} v_{sw} T_p \tag{6}$$

where T_p is the proton temperature in units of Kelvin. For typical solar wind conditions ($v_{sw} = 470\text{kms}^{-1}$ and $T_p = 1.5 \times 10^5\text{K}$), the resulting heating rate is around $2.4\times10^3\text{Jkg}^{-1}\text{s}^{-1}$. After allowing for errors, this is equivalent to approximately 40–60% of the dissipation rate computed from the third-order law. This result is consistent with observations that suggest heating due to turbulence is divided, with 60% going to proton heating and 40% into electron heating [35, 36].

Work has begun on a more detailed and in-depth analysis of the full differential form of the third-order law. This will involve examining some of the more subtle features proposed in different theoretical formulations of the law, and will employ both direct observations and numerical simulations. These results will be presented in a subsequent publication. Finally, parametric or implicit dependence of the third-order law on other turbulence properties will, assuming homogeneity and statistical stationarity, only become important at higher orders in the hierarchy of structure functions. Therefore, we must look to study the more difficult relations that contribute to the highly variable nature of MHD turbulence, and enter beyond the relatively elegant third-order statistics.

The authors are grateful to the Cluster Active Archive for providing the data used in this study. This research is supported in part by the NASA Heliophysics Guest Investigator (NNX09AG31G), NASA Heliophysics Theory (NNX08AI47G) and NSF SHINE (ATM-0752135) Programs. S.D. is a member of CIC (CONICET) and partially supported by grants UBACyT X425, PIP-2009-00825 (CONICET) and PICT 2007-00856 (ANPCyT).

* Electronic address: kto@udel.edu

[1] R. Bruno and V. Carbone, Living Rev. Solar Phys. **2** (2005).
[2] J. Belcher and L. Davis, J. Geophys. Res. **76**, 3534 (1971).
[3] D. Montgomery, Phys. Scr. T. **T2**, 83 (1982).
[4] S. Oughton, E. Priest, and W. Matthaeus, J. Fluid. Mech. **280**, 95 (1994).
[5] K. Osman and T. Horbury, Astrophys. J. **654**, L103 (2007).
[6] A. Kolmogorov, comptes rendus (Doklady) de l'Academie des scienced de l'URSS **32**, 16 (1941).
[7] A. Monin and A. Yaglom, *Statistical Fluid Mechanics: Mechanics of Turbulence*, vol. 2 (M.I.T Press, Cambridge, Mass., 1975).
[8] U. Frisch, *Turbulence* (Cambridge University Press, Cambridge, 1995).
[9] H. Politano and A. Pouquet, Phys. Rev. E **57**, R21 (1998a).
[10] H. Politano and A. Pouquet, Geophys. Res. Lett. **25**, 273 (1998b).
[11] L. Sorriso-Valvo, R. Marino, V. Carbone, A. Noullez, F. Lepreti, P. Veltri, R. Bruno, B. Bavassano, and E. Pietropaolo, Phys. Rev. Lett. **99**, 115001 (2007).
[12] R. Marino, L. Sorriso-Valvo, V. Carbone, A. Noullez, R. Bruno, and B. Bavassano, Astrophys. J. **677**, L71 (2008).
[13] V. Carbone, R. Marino, L. Sorriso-Valvo, A. Noullez, and R. Bruno, Phys. Rev. Lett. **103**, 061102 (2009).
[14] B. MacBride, C. Smith, and M. Forman, Astrophys. J. **679**, 1644 (2008).
[15] J. Stawarz, C. Smith, B. Vasquez, M. Forman, and B. MacBride, Astrophys. J. **713**, 920 (2010).
[16] J. Podesta, Phys. Rev. Lett. **104**, 169001 (2010).
[17] C. Smith, J. Stawarz, B. Vasquez, M. Forman, and B. MacBride, Phys. Rev. Lett. **104**, 169002 (2010).
[18] M. Forman, C. Smith, and B. Vasquez, Phys. Rev. Lett. **104**, 189001 (2010).
[19] L. Sorriso-Valvo, V. Carbone, R. Marino, A. Noullez, R. Bruno, and P. Veltri, Phys. Rev. Lett. **104**, 189002 (2010).
[20] J. Podesta, M. Forman, and C. Smith, Phys. Plasmas **14**, 092305 (2007).
[21] J. Podesta, J. Fluid Mech. **609**, 171 (2008).
[22] M. Wan, S. Oughton, S. Servidio, and W. H. Matthaeus, Phys. Plasmas **16**, 090703 (2009).
[23] S. Galtier, Astrophys. J. **704**, 1371 (2009).
[24] K. Osman and T. Horbury, J. Geophys. Res. **114**, A06103 (2009a).
[25] K. Osman and T. Horbury, Ann. Geophys. **27**, 3019 (2009b).
[26] G. Taylor, Proc. R. Soc. Lond. **164**, 476 (1938).
[27] T. Horbury, in *Cluster 2 workshop on multi-scale/multipoint plasma measurements*, edited by R. Harris (ESA SP-449; Noordwijk: ESA, 2000), pp. 89–97.
[28] A. Balogh, C. Carr, M. Acuna, M. Dunlop, T. Beek, P.Brown, K.-H. Fornacon, E. Georgescu, K. Glassmeier, J. Harris, et al., Ann. Geophys. **19**, 1207 (2001).
[29] H. R. et al., Ann. Geophys. **19**, 1303 (2001).
[30] D. Roberts, M. Goldstein, L. Klein, and W. Matthaeus, J. Geophys. Res. **92**, 12023 (1987).
[31] M. Dobrowolny, A. Mangeney, and P. Veltri, Astron. Astrophys. **83**, 26 (1980).
[32] M. Hossain, P. Gray, D. Pontius, W. Matthaeus, and S. Oughton, Phys. Fluids **7**, 2886 (1995).
[33] P. Coleman, Astrophys. J. **153**, 371 (1968).
[34] B. Vasquez, C. Smith, K. Hamilton, B. MacBride, and R. Leamon, J. Geophys. Res. **112**, A07101 (2007).
[35] B. Breech, W. Matthaeus, S. Cranmer, J. Kasper, and S. Oughton, J. Geophys. Res. **114**, A09103 (2009).
[36] S. Cranmer, W. Matthaeus, B. Breech, and J. Kasper, Astrophys. J. **702**, 1604 (2009).